European Journal of Pharmaceutical Sciences 168 (2022) 106046

Contents lists available at ScienceDirect

European Journal of Pharmaceutical Sciences

journal homepage: www.elsevier.com/locate/ejps

A HET-CAM based vascularized intestine tumor model as a screening platform for nano-formulated photosensitizers

Linda Elberskirch [a], Ronan Le Harzic [a], Dietrich Scheglmann [b], Gerhard Wieland [b], Arno Wiehe [b,c], Maria Mathieu-Gaedke [b,c,1], Hartwig R.A. Golf [b,c], Hagen von Briesen [a], Sylvia Wagner [a,*]

[a] Fraunhofer Institute for Biomedical Engineering, Department Bioprocessing & Bioanalytics, Joseph-von-Fraunhofer-Weg 1, 66280 Sulzbach (Germany)
[b] biolitec research GmbH, Otto-Schott-Strasse 15, 07745 Jena (Germany)
[c] Freie Universität Berlin, Institute for Chemistry and Biochemistry, Takustr. 3, 14195 Berlin (Germany)

ARTICLE INFO

Keywords:
PLGA-nanoparticles
Liposomes
Pharmaceutical test system
Simulated endoscopic irradiation, Angiogenesis

ABSTRACT

The development of new tumor models for anticancer drug screening is a challenge for preclinical research. Conventional cell-based *in vitro* models such as 2D monolayer cell cultures or 3D spheroids allow an initial assessment of the efficacy of drugs but they have a limited prediction to the *in vivo* effectiveness. In contrast, *in vivo* animal models capture the complexity of systemic distribution, accumulation, and degradation of drugs, but visualization of the individual steps is challenging and extracting quantitative data is usually very difficult. Furthermore, there are a variety of ethical concerns related to animal tests. In accordance with the 3Rs principles of Replacement, Reduction and Refinement, alternative test systems should therefore be developed and applied in preclinical research. The Hen's egg test on chorioallantoic membrane (HET-CAM) model provides the generation of vascularized tumor spheroids and therefore, is an ideal test platform which can be used as an intermediate step between *in vitro* analysis and preclinical evaluation *in vivo*. We developed a HET-CAM based intestine tumor model to investigate the accumulation and efficacy of nano-formulated photosensitizers. Irradiation is necessary to activate the phototoxic effect. Due to the good accessibility of the vascularized tumor on the CAM, we have developed a laser irradiation setup to simulate an *in vivo endoscopic* irradiation. The study presents quantitative as well as qualitative data on the accumulation and efficacy of the nano-formulated photosensitizers in a vascularized intestine tumor model.

1. Introduction

Photosensitizers combined with advanced nanotechnology have a great potential for effective cancer treatment (Park et al., 2018). The incorporation of photosensitizers into nanoparticles can help to overcome their major limitations: poor water solubility, long-term phototoxicity and low tumor targeting efficacy (Bae and Na, 2012; Castano et al., 2005; Debele et al., 2015; Park et al., 2018; Zhang et al., 2018). To date, various nanoparticulate incorporated photosensitizers are under development (Bœuf-Muraille et al., 2019; Dinakaran et al., 2020; Mokwena et al., 2018; Shu et al., 2021; Yakavets et al., 2019). Potential new drugs and their formulations are examined in preclinical research for their efficacy and toxicological properties. The aim of preclinical studies is to identify one or more promising drug candidates and provide comprehensive evidence of their efficacy and toxicological safety to conduct *in vivo* studies. The choice of the appropriate test models depends on the disease to be treated and the research question to be investigated. Due to the high number of potential new drugs, screening models are needed which enable a fast and cost-effective investigation of their efficacy and toxicity. Cell-based test systems are an essential element in drug development. Compared to cost-intensive animal models, cell culture-based tests are simple, fast, inexpensive, versatile, and easily to reproduce (Langhans, 2018). Cell cultures with cell lines originating from tumors are most suitable for the development of new cancer drugs. Many cell culture tests used in drug research are 2D monolayer cell cultures where cells are cultivated on flat and inflexible plastic surfaces (Mohs and Greig, 2017). The compound can be incubated for a defined period of time and its biological and toxic effects can

* Corresponding author.
E-mail address: sylvia.wagner@ibmt.fraunhofer.de (S. Wagner).
[1] Present address: Fraunhofer-Institut für Angewandte Polymerforschung IAP, Geiselbergstraße 69, 14476 Potsdam (Germany)

https://doi.org/10.1016/j.ejps.2021.106046
Received 9 May 2021; Received in revised form 15 October 2021; Accepted 15 October 2021
Available online 17 October 2021
0928-0987/© 2021 The Authors. Published by Elsevier B.V. This is an open access article under the CC BY-NC-ND license (http://creativecommons.org/licenses/by-nc-nd/4.0/).

be investigated using standardized tests. These 2D monolayer cell culture systems are suitable for automated high-throughput screening procedures, which enable the initial identification of potential drugs (Lovitt et al., 2014). A disadvantage of 2D monolayer cell cultures are their inability to reproduce the complex physiological conditions of an *in vivo* tumor. Therefore, conclusions about the *in vivo* behavior are difficult to make. With 3D tumor spheroids, the tissue-specific structure of *in vivo* tumors and the resulting physiological conditions can be reflected more realistically (Lovitt et al., 2014). Similar to micro metastases, tumor spheroids with a diameter of more than 500 μm exhibit a physicochemical gradient (Nath and Devi, 2016). This leads to a decrease in the supply of nutrients and oxygen from the surface to the center of the tumor spheroid, while at the same time carbon dioxide and waste products accumulate inside the tumor spheroid. This results in different cell layers within the tumor spheroid, a vital boundary layer with proliferating cells and a nucleus with necrotic cells. Between these layers there is an additional cell layer with cells that are in the quiescent phase and therefore do not proliferate but can be reactivated. The reduced penetration of the drug into the tumor spheroid results in a reduced accessibility of these cells compared to monolayer cell cultures (Lovitt et al., 2014). Studies with 3D tumor spheroids are used in the development of new cancer drugs for selection of effective drugs. Moreover, due to their ability to simulate micro metastases *in vitro*, they can make a contribution to reducing the number of animal experiments (Friedrich et al., 2009). Overall, 3D tumor spheroids can be regarded as an extension to investigations with 2D monolayer cell cultures. However, there are limitations to the transferability of *in vitro* studies to clinical applications (Sausville and Newell, 2004). A major limitation of *in vitro* test systems is the lack of vascularization. The growth of a tumor *in vivo* leads to angiogenesis and thus to a connection to the systemic circulation of the body, which enables the tumor to be provided with nutrients and oxygen (Li et al., 2012). This can have effects on the systemic distribution of drugs or formulations which are scarcely reflected by *in vitro* models. Animal models are usually used to investigate this issue (Lokman et al., 2012; Sausville and Newell, 2004). The use of mice or rats allows the breeding of vascularized *in vivo* tumors. However, the performance of animal experiments is very controversial. *In vivo* studies usually require special skills, approval by the ethics committee, and they are time and cost intensive (Nowak-Sliwinska et al., 2014). In addition, the animal is harmed, and considerable suffering is done, often up to death. In accordance with the 3Rs principles of Replacement, Reduction and Refinement (Russell and Burch, 1959), alternative test systems should therefore be developed and applied in preclinical research (Graham and Prescott, 2015). A promising approach for the investigation of vascularized tumors is the use of the chicken egg test on the chorioallantoic membrane (HET-CAM). The CAM is a highly vascularized membrane responsible for the arterial supply of the embryo. Additionally, immunodeficiency of the chicken embryos allows the application of cells from other species without a reaction of the immune system (Cimpean et al., 2008). After the application of tumor cells to the CAM, angiogenesis and growth of the cell population occurs. The tissue composition and accessibility of CAM for experimental manipulation makes it an excellent preclinical *in ovo* model for drug screening or vascular growth studies (Subauste et al., 2009; Demir et al., 2009; Nowak-Sliwinska et al., 2014). Starting point of the present work was the use of photodynamic therapy (PDT) for the treatment of small intestine carcinomas. The photosensitizer meso-tetra(3-hydroxyphenyl) chlorin (mTHPC) and the newly synthesized photosensitizers BLC 2175 and BLC 5152 were used as drug compounds. Due to the fact, that anti-tumor photosensitizers in general have highly hydrophobic properties, which lead to poor bioavailability and high side effects caused by unspecific systemic accumulation, new formulations based on nanoparticulate drug carrier systems have been developed. The function of the nanoparticle is the transport and release of the photosensitizer at the target site, whereby the specific accumulation at the target site should result in a reduction of side effects at the same time. To study the accumulation and induced phototoxic effects in a vascularized tumor model the HET-CAM assay was used.

2. Methods

2.1. Synthesis and characterization of nanoparticles

2.1.1. Synthesis of photosensitizers blc 2175 and blc 5152

Photosensitizers BLC 2175 and BLC 5152 were synthesized by nucleophilic aromatic substitution on 5,10,15,20-tetrakis(pentafluorophenyl)porphyrin with two amines, 1,3-dihydroxyprop-2-ylamine and (*R*)−2,3-dihydroxyprop-1-ylamine, respectively. 5,10,15,20-Tetrakis (pentafluorophenyl)porphyrin itself was synthesized according to the literature with slight modifications, starting from pyrrole and pentafluorobenzaldehyde using boron trifluoride etherate as the acid catalyst (Geier and Lindsey, 2004; Lindsey et al., 1987).

General procedure for the functionalization of 5,10,15,20-tetrakis (pentafluorophenyl)porphyrin with amines: First, the porphyrin was dissolved in dry DMSO in a three-necked round bottom flask equipped with argon gas inlet and magnetic stirrer. Then, the respective amine was added, and the reaction was stirred for 4 h at 100 °C. After extraction with ethyl acetate and aqueous workup, the organic phase was dried with sodium sulfate, filtered and the solvent evaporated. The crude product was purified by column chromatography (silica gel, DCM/MeOH, 85:15 – 8:2). The product fraction was evaporated to dryness, treated with dichloromethane and suction filtered.

5,10,15,20-Tetrakis-[2,3,5,6-*tetrafluor*-4-(1,3-*dihydroxyprop*-2-*ylamino*)*phenyl*]porphyrin (BLC 2175): Referring to the procedure above, 5,10,15,20-tetrakis(pentafluorophenyl)porphyrin (222 mg, 0.23 mmol) was functionalized with 1,3-dihydroxyprop-2-ylamine (562 mg, 6.17 mmol). The product BLC 2175 was obtained as purple crystals (243 mg, 0.19 mmol, 84%). m. p. 210 °C. ^{1}H NMR (500 MHz, D_6-acetone): δ = 9.25 (s, 8H, β-*H*), 5.29 (s, 4H, N*H*), 4.28 (d, J = 61.2 Hz, 8H, O*H*), 4.16 (t, J = 5.4 Hz, 4H, NHC*H*), 4.09 – 3.93 (m, 16H, OCH_2), −2.82 (s, 4H, $NH_{Pyrrole}$) ppm. ^{13}C NMR (126 MHz, D_6-Acetone): δ = 147.8 (d, $^{1}J_{C\text{-}F}$ = 238.8 Hz, Ar_F-C_{ortho}), 138.3 (dd, $^{1,2}J_{C\text{-}F}$ = 238.8, 16.0 Hz, Ar_F-C_{meta}), 132.7 (β-$C_{Pyrrole}$), 130.5 (t, J = 11.5 Hz, Ar_F-C_{para}), 107.2 (t, $^{2}J_{C\text{-}F}$ = 20.1 Hz, Ar_F-C_{ipso}), 106.0 (Ar_F-C_{meso}), 62.8 (OCH_2), 62.7 (OCH_2), 58.8 (NH—*CH*) ppm. ^{19}F NMR (471 MHz, D_6-acetone): δ = −143.38 (d, J = 16.2 Hz, 4F, Ar-F_{ortho}), −161.31 (d, J = 16.9 Hz, 4F, Ar-F_{meta}) ppm. HRMS (ESI-TOF): *m/z* calc. for $C_{56}H_{43}F_{16}N_8O_8^+$ $[M + H]^+$: 1259.2948; found: 1259.3045. UV/Vis (MeOH): λ_{max} [log ε (L • mol^{-1} • cm^{-1})] = 417 (5.42), 509 (4.38), 544 (3.82), 586 (3.88), 648 (3.07) nm.

5,10,15,20-Tetrakis-[2,3,5,6-*tetrafluor*-4-((*R*)−2,3-*dihydroxyprop*-1-*ylamino*)-*phenyl*]-porphyrin (BLC 5152): Referring to the procedure above, 5,10,15,20-tetrakis(pentafluorophenyl)porphyrin (262 mg, 0.27 mmol) was functionalized with (*R*)−2,3-dihydroxyprop-1-ylamine (529 mg, 5.81 mmol). The product BLC 5152 was obtained as purple crystals (155 mg, 0.12 mmol, 45%). m. p. 298–301 °C. ^{1}H NMR (500 MHz, D_6-acetone): δ = 9.27 (s, 8H, β-*H*), 5.59 (s, 4H, N*H*), 4.40 (s, 4H, O*H*), 4.13 (t, J = 5.8 Hz, 4H, OC*H*), 4.04 (s, 4H, O*H*), 3.95 (dd, J = 12.9, 6.8 Hz, 4H, NHC*H*), 3.78 (d, J = 5.3 Hz, 8H, OCH_2), 3.71 (dt, J = 12.7, 6.3 Hz, 4H, NHC*H*), −2.80 (s, 2H, $NH_{Pyrrole}$) ppm. ^{13}C NMR (126 MHz, D_6-acetone): δ = 147.04 (dd, $J_{C\text{-}F}$ = 247.6, 9.2 Hz, Ar_F-C_{ortho}), 137.45 (dd, $J_{C\text{-}F}$ = 239.8, 17.2 Hz, Ar_F-C_{meta}), 130.37 (t, J = 11.4 Hz, Ar_F-C_{para}), 106.25 (t, J = 20.2 Hz, Ar_F-C_{ipso}), 105.28 (s, Ar_F-C_{meso}), 71.27 (d, OCH), 64.54 (t, OCH_2), 48.66 (t, J = 13.9 Hz, $NHCH_2$) ppm. ^{19}F NMR (471 MHz, D_6-acetone): δ = −143.50 (d, J = 18.7 Hz, 4F, Ar-F_{ortho}), −161.91 (d, J = 19.8 Hz, 4F, Ar-F_{meta}) ppm. HRMS (ESI-TOF): *m/z* calc. for $C_{56}H_{43}F_{16}N_8O_8^+$ $[M + H]^+$: 1259.2948; found: 1259.2946. UV/Vis (MeOH): λ_{max} [log ε (L • mol^{-1} • cm^{-1})] = 417 (5.27), 510 (4.23), 543 (3.75), 586 (3.78), 648 (3.16).

2.1.2. Liposome based nanoparticles

Liposomes were prepared by the conventional film method as a 9:1 mixture of dipalmitoylphosphatidylcholine (DPPC) and

dipalmitoylphosphatidylglycerol (DPPG). The photosensitizer was dissolved in an organic solution of phospholipids (chloroform/methanol 3:2 (v/v)). This mixture was dried to a thin film at 50 °C using the rotary evaporator. The obtained film was kept under vacuum (1 mbar) for 2 h at room temperature. The film was then hydrated for 30 min. Afterwards the liposome dispersion was extruded through polycarbonate membranes of different pore sizes (400 nm, 200 nm, 100 nm). Liposomal size was measured by Photon Correlation Spectroscopy (PCS) with a Zetasizer Nano S90 from Malvern Instruments GmbH (Herrenberg, Germany). Photosensitizer concentration was determined by UV–Vis spectroscopy.

2.1.3. PLGA based nanoparticles

Two kinds of nanoparticles with muco-adhesion and –permeating properties have been produced by the modification of the nanoparticle surface as previously described (Elberskirch et al., 2021). The first particle system, termed as NP-PLGA-mTHPC—CP (poly(lactide-co-glycolide)-Carbopol®), was produced by means of solvent evaporation. The protocols according to Rojnik et al. (Rojnik et al., 2012) and Niu et al. (Niu et al., 2009) served as the basis for the development of the synthesis protocol. For the aqueous phase, a 0.1% Carbopol® (Lubrizol, Hamburg, Germany) stock solution was prepared with ultrapure water and left to swell overnight. The stock solution was then adjusted to pH 7 using 2 M sodium hydroxide (Sigma-Aldrich GmbH, Steinheim, Germany). Then, 100 µL of 10% hydrochloric acid (Sigma-Aldrich GmbH, Steinheim, Germany) were added to reduce the increased viscosity of the mixture. The pH value was then adjusted for neutralization by adding 2 M sodium hydroxide solution and autoclaved. To prepare the organic phase, 20 mg resomer RG 503 H (Sigma-Aldrich GmbH, Steinheim, Germany) was dissolved in 1 ml DMSO (Sigma-Aldrich GmbH, Steinheim, Germany). The organic solution was added dropwise at a rate of 0.5 ml min^{-1} into a 0.04% carbopol-water phase while stirring at 600 rpm. To produce the mTHPC incorporated nanoparticles, the photosensitizer mTHPC was dissolved in the organic phase at a concentration of 0.25 mg ml^{-1}. To evaporate the solvent, the emulsion was stirred for at least 5 h. The nanoparticles were purified by centrifugation for 30 min at 21,000 x g and a temperature of 4 °C. The supernatants were discarded, and the pellet resuspended in PBS. The second particle system called NP-PLGA-mTHPC-F127 (poly(lactide-co-glycolide)-Polaxamer 407) was synthesized according to a modified protocol of Xu et al. (Xu et al., 2013). The method is described as W/O/W double emulsion solvent evaporation process. An oil phase consisting of a mixture of 1 ml acetone (Sigma-Aldrich GmbH, Steinheim, Germany), 3 ml dichloromethane (DCM) (Sigma-Aldrich GmbH, Steinheim, Germany) and 50 mg PLGA was prepared. For the incorporation of the photosensitizer an additional 0.5 mg mTHPC was dissolved in the oil phase. This solution was homogenized by using an ultrasonic homogenizer at an amplitude of 30% for 30 s. A second solution of 10 ml 1% saponin solution (Sigma-Aldrich GmbH, Steinheim, Germany) was added as an aqueous phase and the oil phase was pipetted in rapidly dropwise. The resulting double emulsion was further homogenized at an amplitude of 70% for 5 min. This was pipetted dropwise while stirring at 800 rpm to a further 1% saponin solution with a volume of 30 ml. The containing dichloromethane and acetone were evaporated for three hours while stirring at 800 rpm and then placed in a desiccator under vacuum overnight. The nanoparticles were purified by centrifugation at 21,000 x g for 30 min. The supernatant was discarded, and the pellet resuspended in sterile ultrapure water. Purification was repeated twice. To modify the nanoparticles, a 0.1% F127 (Sigma-Aldrich GmbH, Steinheim, Germany) solution was used to resuspend the pellets during purification. The adsorption is achieved by hydrophobic interactions that form between the poly(propylene oxide) block (PPO block) of F127 and PLGA. Nanoparticles were stored at 4 °C until usage. Nanoparticle size, polydispersity index and zeta potential were determined using a Zetasizer Nano ZS (Malvern Panalytical GmbH, Herrenberg, Germany) and photosensitizer concentration was quantified by HPLC analysis.

2.2. Preclinical studies

2.2.1. Tumor spheroid generation

The generation of the tumor spheroids was done by following a previously described protocol (Elberskirch et al., 2021). The duodenum adenocarcinoma cell line HuTu-80 (CLS Cell Lines Service GmbH, Eppelheim, Germany) and the human colon cancer cell line HT29-MTX-E12 (European Collection of Cell Cultures (ECACC)) were used for the generation of the tumor spheroids. The cells were cultured at 37 °C, 5% CO_2 and 95% relative humidity in an incubator. The HuTu-80 culture medium EMEM (CLS Cell Lines Service GmbH, Eppelheim, Germany) was supplemented with 10% foetal bovine serum (Sigma-Aldrich GmbH, Steinheim, Germany) and antibiotics (1% Penicillin-Streptomycin, 10,000 U ml^{-1}, Invitrogen GmbH). The used culture medium DMEM for the HT29-MTX-E12 cells was supplemented with 2 mM glutamine, 1% non-essential amino acids (all purchased from Life Technologies GmbH, Darmstadt, Germany), antibiotics (1% Penicillin-Streptomycin, 10,000 U ml^{-1}, Invitrogen GmbH) and 10% foetal bovine serum (Sigma-Aldrich GmbH, Steinheim, Germany) and the cells were grown until 70–80% confluence. For the generation of the tumor spheroids, 4500 cells per well were seeded in corning spheroid microplate (Corning, Wiesbaden, Germany) and cultured over five days with changing of medium every second day. On day five, the spheroids were transferred to a Cero cell culture tube and cultured under rotating conditions in a Cero (both purchased from OLS OMNI Life Science, Bremen, Germany). On day ten, batches of five spheroids were transferred to a 24-well cell suspension multiwell plate (Greiner Bio-One, Frickenhausen, Germany) and cultured under static conditions for two days until they build out a necrotic core. The resulting tumor spheroids were applied to the CAM within three days.

2.2.2. HET-CAM

Fertilized chicken eggs (LSL Rhein-Main GmbH & Co. KG, Dieburg, Germany) were used for the HET-CAM test. They were stored at 16 °C for three days after delivery to recover from the shocks of transport. As a basis for establishing the method, the protocol of Zabielska-Koczywas et al. (Zabielska-Koczywas et al., 2017) was used and modified (Fig. 1). The incubation of the eggs was started by transferring them to an incubator. The eggs were incubated with the blunt end pointing upwards for three days at 37.5 °C, 65% humidity and an inclination of 120° Additionally, they were turned 3 times a day to simulate natural incubation conditions. On the third day of incubation a hole was drilled into the blunt end of each egg and covered with adhesive tape. The eggs were further incubated for two days (37.5 °C, 65% humidity, inclination 11° every 2 h) with the blunt ends pointing downwards. On the 5th day of incubation, a second hole was drilled into the pointed end of each egg. To move the air bubble from the blunt end to the pointed end, the tape was taken off the blunt end. By slightly tilting the egg, the CAM detaches from the shell and shell skin in the area of the pointed end through pressure equalization and air inflow. This allows the egg to be opened without risk of damaging the CAM. A circular window with a diameter of about 1 cm was carefully drilled into the pointed end of the eggs with a circular saw without damaging the shell membrane. The eggshell and the shell membrane were removed from the window with tweezers. The opened eggs were sealed with a plastic foil and incubated for 24 h in an incubator (37.5 °C, 65% humidity) without tilting. On the 6th day of incubation, the HuTu-80 and HT29-MTX-E12 tumor spheroids were applied to the CAM. In this step, five tumor spheroids per CAM were applied to the CAM using a pipette. The vitality and the development of the chick embryos as well as the angiogenesis of the tumor spheroids was monitored with a microscope (SZX16, Olympus Europa SE & Co. KG, Germany). About 70% of the eggs showed successful angiogenesis and growth of the applied tumor spheroids. These were treated with the free and nanoparticulate photosensitizers on day 12. These were previously diluted to a concentration of 5 µmol l^{-1} in cell-specific medium. A volume of 100 µl of the sample solutions were slowly dropped with a

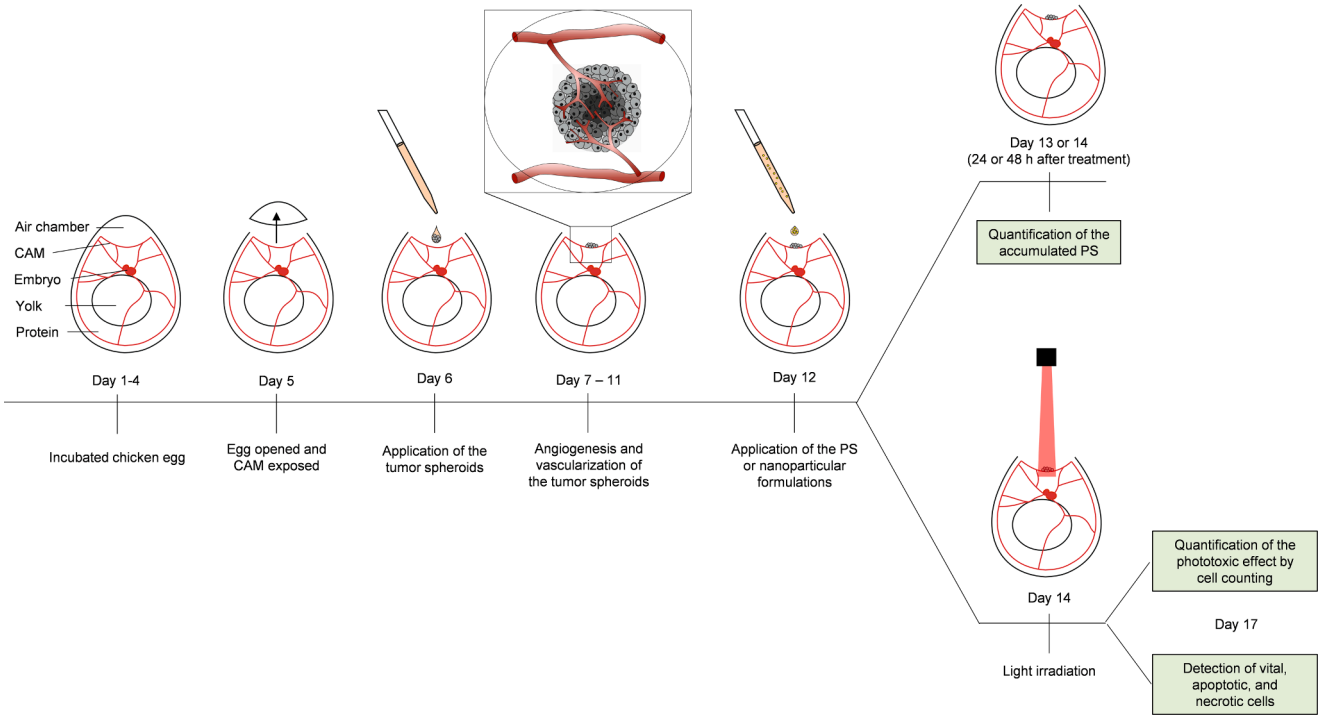

Fig. 1. Schematic drawing of the HET-CAM assay procedure The schematic drawing of an incubated chicken egg shows the air chamber, the chorioallantoic membrane (CAM), the embryo, the yolk and protein. The egg was opened on day 5 to expose the CAM. Application of the tumor spheroids was done on day 6 by direct application onto CAM. After application of tumor spheroids follows angiogenesis and vascularization (day 7–11). The PS or nanoparticular formulations were applied on day 12 followed by quantification of the accumulated PS on day 13 and 14 or light irradiation and quantification of the phototoxic effect by cell counting or detection of vital, apoptotic, and necrotic cells on day 17.

pipette onto the surface of the tumor spheroid. After an incubation period of 24 h or 48 h, respectively, the amount of the accumulated photosensitizers in the tumor spheroid and the induced phototoxic effect were investigated in different experimental approaches. On the 17th day of development, the experiments were stopped by decapitation of the embryos.

2.2.3. Evaluation of dark toxicity

To evaluate the dark toxic effects of the photosensitizer in the HET-CAM assay, studies on the dark toxic effects of the photosensitizer with mTHPC were performed. For this purpose, vascularized tumor spheroids of the cell lines HuTu-80 an HT29-MTX-E12 were incubated with 5 µmol l^{-1} of the free photosensitizer mTHPC for 48 h on day 12 and not irradiated. An optical control was performed on day 17. Regarding the conversation of the fertilized chicken eggs, the dark toxicity of the photosensitizers BLC 2175, BLC 5152 and nanoparticulate formulations of the photosensitizer LP-BLC 2175, LP-BLC 5152, NP-PLGA-mTHPC—CP and NP-PLGA-mTHPC-F127 was investigated in preliminary studies using tumor spheroids of the cell lines HuTu-80 an HT29-MTX-E12, which were incubated with 5 µmol l^{-1} of the corresponding photosensitizer in 96-well plates. The viability was measured by the alamarBlue™ (Invitrogen GmbH, Karlsruhe, Germany) assay and the effect of the photosensitizers and nanoparticulate formulations of the photosensitizer was compared to untreated tumor spheroids.

2.2.4. Scanning electron microscope images

To characterize the morphology and surface of the tumor spheroids, these were prepared for scanning electron microscopy in accordance to the protocol of Katsen et al. (Katsen-Globa et al., 2016; Katsen et al., 1998). Therefore, untreated tumor spheroids were transferred to Transwell® cell culture inserts (Corning, Germany), washed in PBS and were fixed overnight in 2% glutaraldehyde in 0.1 M sodium cacodylate buffer. A post fixation followed by using a 2% osmium tetroxide solution prepared in sodium cacodylate buffer. The samples were dehydrated by using an increasing series of ethanol solutions (10%, 20%, 30%, 40%, 50%, 60%, 70%, 80%, 90%, and 100%). The samples were coated with carbon and examined with a scanning electron microscope (EVO MA 10, Zeiss).

2.2.5. Construction of the light irradiation setup

A specific irradiation unit was built for the irradiation of vascularized tumor spheroids. For this purpose, a cost-effective compact (Ø 5.6 mm TO can) continuously wave (CW) stable laser diode with a wavelength of 635 nm and 30 mW output power was used (Laser components GmbH, Germany). An aspherical lens with an effective focus length of 9 mm was used to collimate and slightly focus the laser beam and hence reduce the high divergence and spherical aberrations of such a laser diode. An iris diaphragm was introduced in the laser beam pathway to control and vary the irradiation area and the amount of laser power as well. The distance can be varied to refine the size of the laser spot on the irradiation area. A portable laser beam and spectral measurement device (LaserCheck™, Melles Griot GmbH, Germany) was used to measure the emitted light power (mW) and thus deduce the time required to reach a desired irradiation dose (J cm^{-2}) depending on the size of the irradiated area.

2.2.6. Cell separation and counting of vascularized tumor spheroids

After treatment of the vascularized tumor spheroids, they were extracted from the CAM on day 17 and transferred to sampling tubes (Eppendorf AG, Hamburg, Germany). The cells were separated by adding 1 ml trypsin/EDTA (Invitrogen GmbH, Karlsruhe, Germany) within 5 to 30 min on a thermo mixer (Eppendorf AG, Hamburg, Germany) at 37 °C, followed by centrifugation for 5 min at 115 x g and resuspension of the cell pellets in 1 ml PBS (Invitrogen GmbH, Karlsruhe, Germany). Further steps were performed according to the manufacturer's instructions. After the washing steps, the cells were counted using CASY®

TT cell counter (OLS OMNI Life Science GmbH & Co KG, Bremen, Germany).

2.2.7. Quantification of the photosensitizers

The analysis of the photosensitizers mTHPC and the newly synthesized photosensitizers BLC 2175 and BLC 5152 was performed with an Agilent 1260 Infinity Quarternary liquid chromatography (LC) System (Agilent Technologies, Germany), equipped with a diode array detector (DAD). The separation was carried out at 60 °C on a reversed-phase column (Agilent InfinityLab Poroshell 120 EC—C18, 2,1 × 100 mm, 2,7 µm LC-column), which was connected with a guard column (Agilent InfinityLab Poroshell 120 EC—C18, 2.1 × 5 mm, particle size 2.7 µm). The elution was performed with a gradient of solvent A (water), solvent B (acetonitrile) and solvent C (0.1% trifluoracetic acid in water) as follows: 0–0.5 min, 76.5% of A, 8.5% of B, 15% of C; 0.5–2.5 min, 42.0% of A, 38.0% of B, 20.0% of C; 2.5–4 min, 0% of A, 57.5% of B, 42.5% of C; 4–10 min 0% of A, 57.5% of B, 42.5% of C and 10–14 min 76.5% of A, 8.5% of B, 15% of C. The flow rate was 0.4 ml min^{-1}, the injection volume was 2 µl and the measurement was performed at a wavelength of 415 nm.

2.2.8. Detection of apoptotic and necrotic events

The main reactions triggered by PDT in tumor cells are apoptosis and necrosis. Detecting these provides information about the cellular composition of vascularized tumor spheroids according to the induced phototoxicity. Detection was performed with the eBioscience™ Annexin V Apoptosis Detection Kit (Thermo Fisher Scientific GmbH, Dreieich, Germany) in combination with flow cytometric measurements. Measurements were performed with vascularized HuTu-80 and HT29-MTX-E12 tumor spheroids treated with 5 µmol l^{-1} mTHPC and 5 µmol l^{-1} nanoparticulate formulations. After 48 h incubation time the vascularized tumor spheroids were irradiated with about 50 J cm^{-2}. An untreated cell control was included in each examination. 72 h after irradiation, the vascularized tumor spheroids were extracted from the CAM and separated following section 2.3.5. The separated cell were diluted to a concentration of 5×10^6 cells ml^{-1} in the binding buffer of the kit. 5 µl were added to the FITC-conjugated Annexin V solution per 100 µl cell suspension and incubated for 15 min at room temperature. The cells were then washed and resuspended again with 200 µl binding buffer. Then 5 µl propidium iodide solution was added. The samples were transferred to sample tubes (Becton Dickinson GmbH, Heidelberg, Germany) and measured within 4 h by flow cytometry FACSCalibur™ (Becton Dickinson GmbH, Heidelberg, Germany). Per sample 10,000 cells were counted, analyzed, and evaluated with the CellQuest™ Pro-software (Becton Dickinson GmbH, Heidelberg, Germany). Apoptotic cells were identified by green fluorescence, necrotic cells by red fluorescence and vital cells were evaluated as non-fluorescent cells.

2.4. Statistical analysis

The results were presented as mean ± standard deviation. A comparison of the quantified free mTHPC and photosensitizer incorporated into the nanoparticles was performed using the Welch *t*-test. P values < 0.05 were considered as statistically significant.

3. Results and discussion

3.1. Characterization of liposome and plga based nanoparticles

Liposome size and polydispersity index (PDI) were measured for characterization. The liposomes LP-BLC 2175 had a mean size of 151.6 ± 2.3 nm with a PDI of 0.189 ± 0.03 and liposomes LP-BLC 5152 144.3 ± 1.9 nm with a PDI of 0.175 ± 0.02. Two synthesis methods were used for the preparation of PLGA based nanoparticles, the nanoprecipitation and double emulsion solvent evaporation. The particle size, PDI and zeta potential were measured for characterization. The PLGA based nanoparticles NP-PLGA-mTHPC—CP had a mean size of 124.1 ± 2.8 nm, a PDI of 0.03 ± 0.01 and a zeta potential of - 52.8 ± 1.5 mV. The F127-mTHPC-PLGA had a mean size of 115,4 ± 0,8 nm, a PDI of 0,09 ± 0,01 a zeta potential of - 46,5 ± 4,5 mV.

3.2. Vascularized tumor spheroid model

The process of tumor spheroid angiogenesis was monitored with microscopic investigation. After the application of five tumor spheroids on day six, the tumor spheroids grow together, and form one tumor spheroid followed by vascularization on day seven to ten (Fig. 2). To visualize the tumor spheroid vascularization scanning electron microscopic images of a vascularized HuTu-80 tumor spheroid were done on day 17 (Fig. 3). The *in ovo* brightfield image showed a white tumor spheroid surrounded by large and small blood vessels with a diameter of approximately 4 mm (Fig. 3, A). The scanning electron microscopic images of the CAM make the vascularization visible. A large blood vessel could be seen from which several blood vessels of different sizes branched off (Fig. 3, B and C). On the tumor spheroid itself, both blood vessels surrounded by the cells of the tumor spheroid and blood vessels growing into the tumor spheroid from the outside could be detected (Fig. 3, D and E).

Tumor angiogenesis represents a critical step in the development of a tumor. Before the development of blood vessels, the tumor is in a resting stage where there is a balance between cell proliferation and cell death. In this stage, the tumor cannot grow and is micro-sized. Angiogenesis leads to the formation of blood vessels that supply the tumor with oxygen and nutrients, which results in growth of the tumor (Lebelt et al., 2008). The influence of a systemic circulation on the accumulation of a drug cannot be investigated with standardized *in vitro* models, therefore animal models are usually used to answer this question. However, these models are very time-consuming, costly and should be critically reviewed with regards to animal welfare (Langhans, 2018). The hen's egg test on the chorioallantoic membrane (HET-CAM) or the tumor chorioallantoic membrane model can be regarded as a link between standardized screening models and animal models. The HET-CAM model is often used to study the angiogenesis of tumor cells and the effectiveness of anticancer drugs (Manjunathan and Ragunathan, 2015; Nowak-Sliwinska et al., 2014; Ribatti et al., 1997; Swadi et al., 2018; Vu et al., 2018; Xiao et al., 2015). The model has several advantages, including a highly vascularized membrane that promotes tumor cell angiogenesis, high reproducibility, and simple and cost-effective experimental design.

3.3. Quantification of the accumulated photosensitizer

An important factor for the effectiveness of PDT is the accumulation of the photosensitizer in the tumor tissue. For this purpose, 100 µl solution (5 µmol l^{-1}) of the photosensitizer as free compound or incorporated in nanoparticle were pipetted directly onto the vascularized tumor spheroids. After an incubation period of 24 h or 48 h, the tumor spheroids were removed from the CAM, the photosensitizer was purified from the cell lysate and measured by HPLC. For calculation of the accumulated amount of the photosensitizer, the mean value from four independent HET-CAM experiments was used, which in turn correspond to four individual vascularized tumor spheroids. The accumulation of mTHPC and the nanoparticular formulations were compared by statistical analysis. The nanoparticular formulations LP-BLC 2175, LP-BLC 5152 and NP-PLGA-mTHPC—CP show a comparable accumulation to mTHPC. The accumulation of the nanoparticular formulation F127-mTHPC-PLGA is significantly higher compared to the free compound mTHPC. A comparison of the 24 h and 48 h incubation time of the free and nanoparticulate incorporated photosensitizers showed for the vascularized tumor spheroids of the cell line HuTu-80 after 48 h an increased accumulation of 97% for mTHPC, 56% for LP-BLC 2175, 46% for LP-BLC 5152, 50% for NP-PLGA-mTHPC—CP and 20% for NP-PLGA-

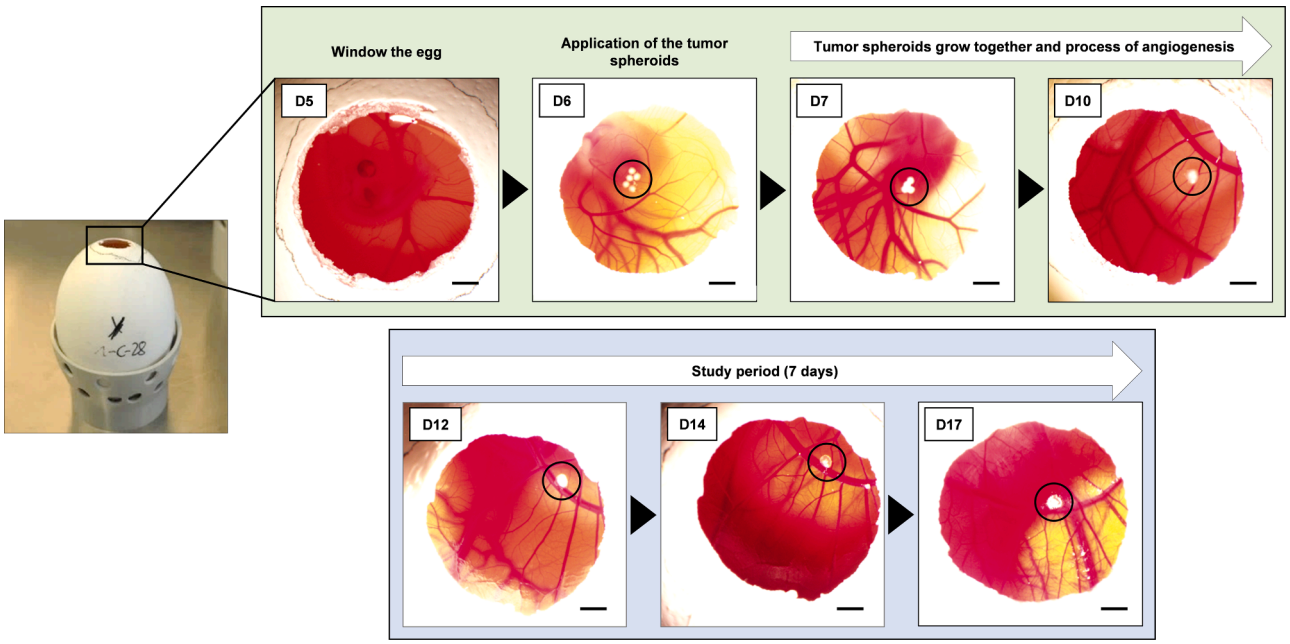

Fig. 2. Microscopic investigation of the tumor spheroid application The different stages of the HET-CAM tumor spheroid model are presented by tumor spheroids of the HuTu-80 cell line. On day 5 (D5), the egg is opened and on day 6 (D6), five tumor spheroids were applied. The fusion and vascularization of the individual tumor spheroids occurs in the period between day 7 - 10 (D7 - D10). The resulting study period was 7 days (D12 - D17). On day 17 (T17) the experimental period ends. (Scale bar 2 mm).

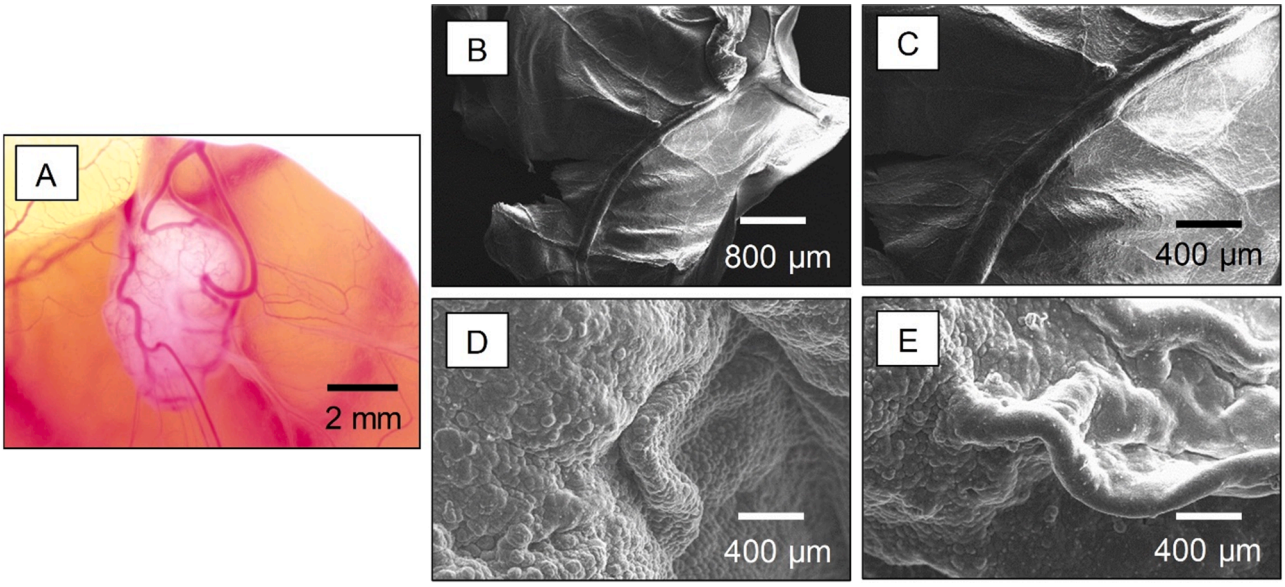

Fig. 3. Microscopic images of a vascularized tumor spheroid on CAM Figure A) Shown is a HuTu-80 tumor spheroid on day 17 in the egg visualized by light microscopy. The tumor spheroid was extracted from the egg and examined by scanning electron microscopy. Figure B) and C) show the vascularized CAM by scanning electron microscopy. Figure D) shows a blood vessel surrounded by the cells of the tumor spheroid by scanning electron microscopy. Figure E) shows a blood vessel that has grown into the tumor from the outside by scanning electron microscopy.

mTHPC-F127 (Fig. 4, A). The vascularized tumor spheroids of the cell line HT29-MTX-E12 also showed an increased accumulation for the nanoparticulate formulations after 48 h compared to the 24 h incubation of 26% for LP-BLC 2175, 46% for LP-BLC 5152, 39% for NP-PLGA-mTHPC—CP and 18% for NP-PLGA-mTHPC-F127 (Fig. 4, B). Overall, a 48 h incubation period of free and nanoparticulate formulations of the photosensitizers caused an increased accumulation inside the tumor spheroids. Therefore, an incubation period of 48 h was used for the investigation of the phototoxic effect.

A crucial factor for the effectiveness of the photodynamic therapy is the accumulation of the photosensitizer in the tumor tissue (Castano et al., 2004). Effective transport is closely related to the angiogenesis of a tumor to the vascular system of the body. (Dewhirst and Secomb, 2017). *In vitro* assays provide an initial platform for cancer drug discovery approaches nevertheless they are limited by the inability of vascularization. Therefore, the HET-CAM model combined with tumor spheroids is an excellent test system to study the accumulation of drugs into vascularized tumor spheroids (Vargas et al., 2007). Considering the procedure in the clinical application of PDT, radiation is performed 24 h to 96 h after the administration of the photosensitizer. This time period is

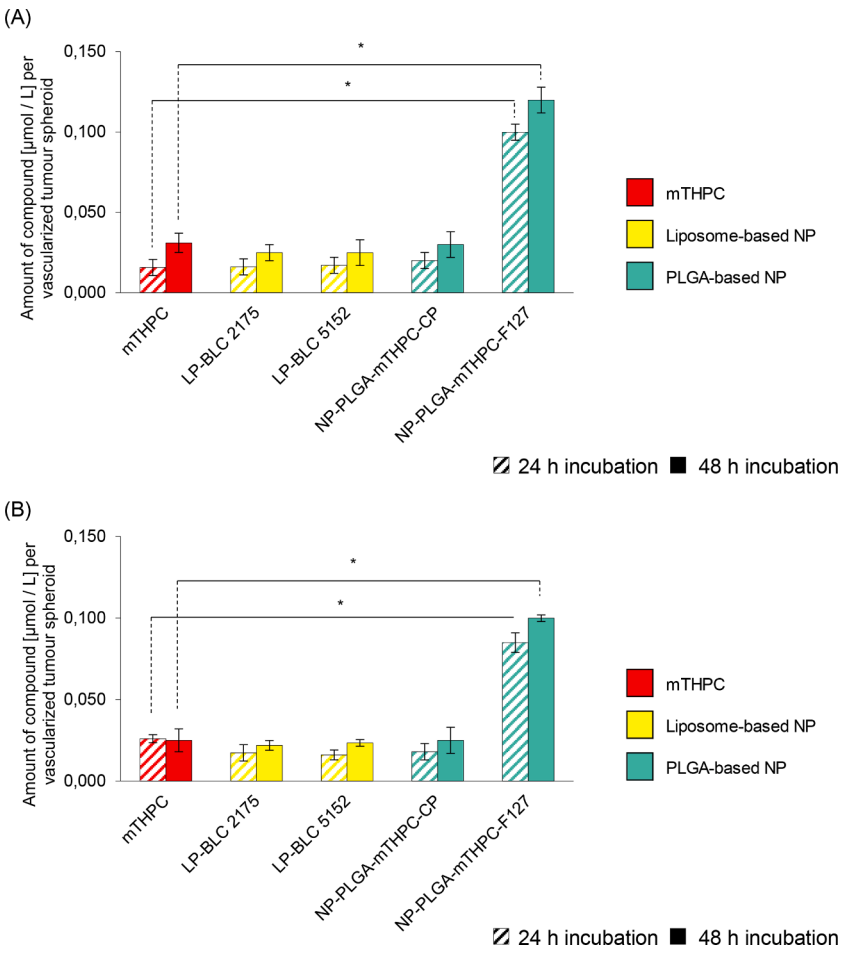

Fig. 4. Quantification of the accumulated photosensitizer in vascularized tumor spheroids of the cell line HuTu-80 and HT29-MTX-E12 after 24 h or 48 h incubation The free compound mTHPC and the nanoparticulate formulations LP-BLC 2175, LP-BLC 5152, NP-PLGA-mTHPC—CP and NP-PLGA-mTHPC-F127 were incubated on vascularized tumor spheroids of the cell line (A) HuTu-80 and (B) HT29-mTX-E12 for 24 h and 48 h respectively. Afterwards, the tumor spheroids were lysed and the photosensitizer was extracted. The amount of the photosensitizer in the vascularized tumor spheroids was detected by HPLC analysis. The results are presented as mean value ± standard deviation. *Significant deviation of the measured values of the liposomal and nanoparticulate formulations compared to the free photosensitizer mTHPC according to the Welch-Test with a significance level of 5% ($n = 4$; $k = 4$).

related to the specific accumulation of the photosensitizer in the tumor tissue (Cramers et al., 2003). Analogous to the clinical application of PDT the investigation of free mTHPC and nanoparticulate photosensitizers also revealed a correlation between the accumulated amount of compound and the incubation time in the vascularized tumor spheroid. In contrast, in a study by Kiesslich et al. with mTHPC a solvent-based formulation (Foscan®) and a liposomal formulation (Foslip®) were incubated on monolayer cell culture of a human gall bladder cancer cell line and a human bile duct cancer cell line until 36 h. After an incubation period of 20 h the accumulation of the photosensitizers approaches a plateau phase (Kiesslich et al., 2007). The result of this study is not consistent with the situation *in vivo* and may lead to a misinterpretation of the necessary incubation time of drugs for following *in vivo* studies or further clinical applications. The example demonstrates that an advanced test system like the HET-CAM model is necessary and appropriate to improve the predictability and transferability of results to the *in vivo* situation.

3.4. Evaluation of dark toxicity

The vascularized tumor spheroids of the cell lines HuTu-80 and HT29-MTX-E12 incubated with the free mTHPC showed no optical changes compared with the untreated and non-irradiated control. It was concluded that no dark toxic effect occurred when the free photosensitizer was used for incubation at a concentration of 5 µmol l^{-1} for 48 h. The dark toxicity of the photosensitizers BLC 2175, BLC 5152 and nanoparticulate formulations of the photosensitizer LP-BLC 2175, LP-BLC 5152, NP-PLGA-mTHPC—CP and NP-PLGA-mTHPC-F127 was investigated in preliminary studies using tumor spheroids of the cell lines HuTu-80 an HT29-MTX-E12. The measurement of the viability showed no effect compared to the untreated control (data not shown). It was concluded that the photosensitizers BLC 2175, BLC 5152 and nanoparticulate formulations of the photosensitizer LP-BLC 2175, LP-BLC 5152, NP-PLGA-mTHPC—CP and NP-PLGA-mTHPC-F127 have no dark toxic effect.

3.5. Light irradiation unit and parameters

In order to activate the photosensitizer, an irradiation unit was built, which enabled the focused irradiation of the vascularized tumor spheroid on the CAM of the incubated chicken egg (Fig. 5). Determination of the phototoxic effect of free and particulate formulations requires irradiation with light of a suitable wavelength. The used photosensitizer mTHPC has a main absorption peak at ~415 nm (Soret band) and multiple absorption peaks between 500 and 700 nm Q-bands) (Bonnett et al., 1989; Ma et al., 1994). For clinical applications, a longer wavelength light source is preferred due to the deeper penetration depth of this light in tissue (Ana P Castano et al., 2004). Results of *in vitro* and *in vivo* studies have shown that mTHPC absorbs significantly at 652 nm which is therefore the commonly used wavelength for the induction of the phototoxic effect. Based on this, a laser diode with a main peak of 635 nm was chosen for the customized light irradiation unit. Based on internal experience and literature data (Betz et al., 2008; Hornung et al., 2004), an irradiation dose of about 50 J cm^{-2} has to be reached. The vascularized tumor spheroids were continuously irradiated with a laser power of 10 mW on a surface area of 0.3 cm^2 during 8 to 9 min, which corresponds thereby to a fluence between 48 J cm^{-2} and 54 J cm^{-2}. The following results obtained here suggest that sufficient effectiveness was achieved with the customized irradiation unit and the parameters chosen.

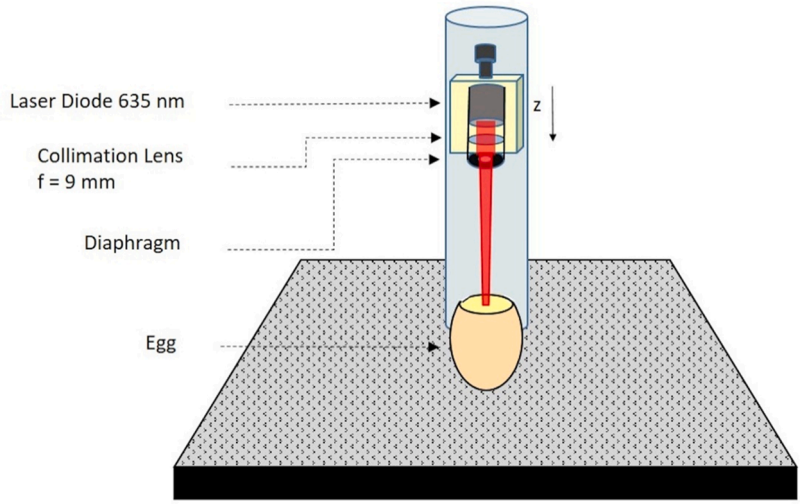

Fig. 5. Experimental setup schematic drawing of the irradiation unit for the vascularized tumor spheroids The developed irradiation unit enables the irradiation of vascularized tumor spheroids *in ovo* at a wavelength of 635 nm. The main components of the irradiation unit are a laser diode, a collimation lens, and an iris diaphragm.

3.6. Quantification of the phototoxic effect by cell counting

The tumor size after treatment was determined to quantify the anti-tumor phototoxic effect of the free and nanoparticulate formulations of the photosensitizer. This was done by cell counting of the tumor spheroids on day 17 of the HET-CAM test. Vascularized tumor spheroids of the cell lines HuTu-80 and HT29-MTX-E12 on day 12 were incubated with 5 µmol l^{-1} of free mTHPC and the nanoparticulate formulations for 48 h. On day 14, irradiation of the vascularized tumor spheroids was performed. Afterwards the vascularized tumor spheroids were extracted by the CAM on day 17 and the cells were separated and counted. An untreated tumor spheroid control was included as reference value and cell count was normalized to 100%. For the cell line HuTu-80 the cell count of $1.97 \times 10^5 \pm 0.31 \times 10^5$ was normalized to 100 ± 16% and for

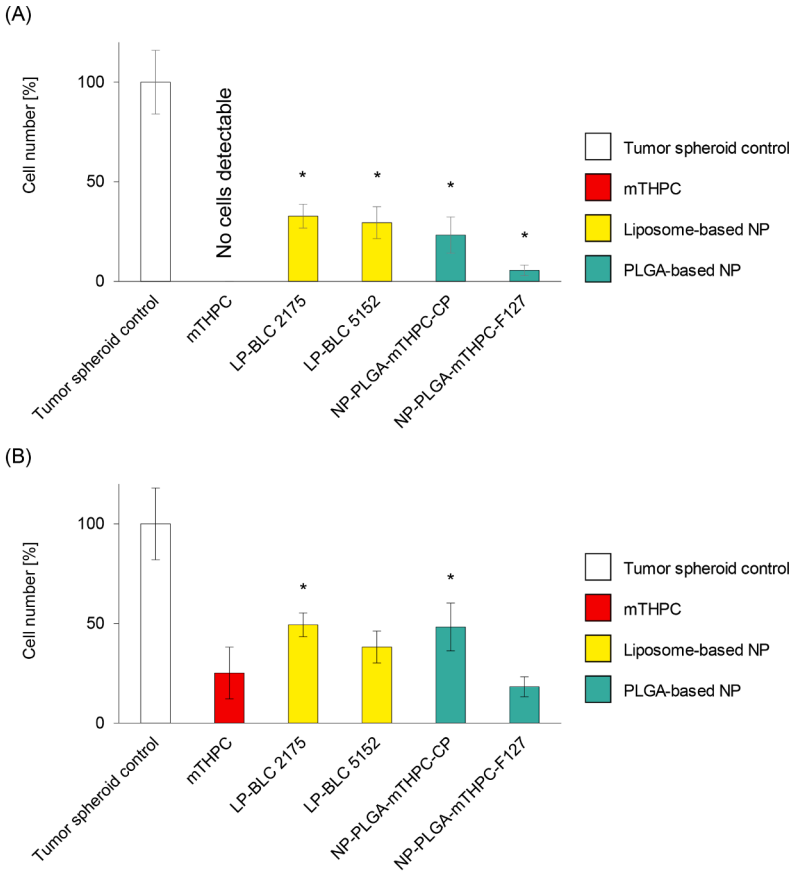

Fig. 6. Quantification of the cell number of the vascularized tumor spheroids of the cell line HuTu-80 and HT29-MTX-E12 after incubation and irradiation The diagram shows the measured cell number (%) of the vascularized tumor spheroids of the cell line HuTu-80 (A) and HT29-MTX-E12 (B) after 48 h incubation with the free photosensitizer mTHPC, the liposome-based nanoparticles LP-BLC 2175 and LP-BLC 5152, and the PLGA-based nanoparticles NP-PLGA-mTHPC—CP and NP-PLGA-mTHPC-F127 compared to the untreated tumor spheroid control, which was also irradiated. The concentration of the photosensitizers was 5 µmol l^{-1}. The results are given as mean value ± standard deviation is represented. *Significant deviation of the relative values of the liposomal and nanoparticulate formulations compared to the free photosensitizer mTHPC according to the Welch-Test with a significance level of 5% ($n = 4$; k = 4).

1

the cell line HT29-MTX-E12 the cell count of $2.28 \times 10^5 \pm 0.41 \times 10^5$ was normalized to 100 ± 18%. Accordingly, the determined cell counts of the vascularized tumor spheroids treated with free and nanoparticulate photosensitizer were calculated in percentage for comparison. After the treatment of the vascularized HuTu-80 tumor spheroids with the free photosensitizer mTHPC no more tumor cells could be detected on the CAM. The treatment with the nanoparticulate formulations of the photosensitizer resulted in a reduction of the cell count to 33 ± 6% for LP-BLC 2175, to 29 ± 8% for LP-BLC 5152, to 23 ± 9% for NP-PLGA-mTHPC—CP, and to 6 ± 3% for NP-PLGA-mTHPC-F127 (Fig. 6) compared to the cell control. Correspondingly, a reduction of the cell number of the vascularized HT29-MTX-E12 tumor spheroids to 25 ± 13% for the free photosensitizer mTHPC was observed. For the liposome-based nanoparticles the values were 49 ± 6% for LP-BLC 2175 and 38 ± 8% for LP-BLC 5152. The PLGA-based nanoparticles were observed to reduce the size of the tumor spheroid after treatment to 48 ± 12% for NP-PLGA-mTHPC—CP and to 18 ± 5% for NP-PLGA-mTHPC-F127. Comparing the number of counted cells after treatment of the vascularized tumor spheroids with the nanoparticular formulations of the PS, the cell numbers of the cell line HuTu-80 differ significantly. The vascularized tumor spheroids HT29-MTX-E12, treated with the nanoparticulate formulations LP-BLC 2175 and NP-PLGA-mTHPC—CP, show a significantly higher cell number compared to the free photosensitizer mTHPC. This result indicates that the effectiveness in terms of reduced number of tumor cells with the nanoparticulate formulations LP-BLC 5152 and NP-PLGA-mTHPC-F127 was comparable to the free photosensitizer mTHPC.

A reduction in tumor size could be demonstrated after treatment with the free photosensitizer mTHPC and the nanoparticulate formulations. In clinical application, tumor size is an important factor in assessing the effectiveness of treatment. For example, in the routine treatment of head and neck tumors with PDT, a reduction of the tumor between 85% and 96% is expected after two applications (Biel, 2010; Lou et al., 2003). After treatment of the vascularized tumor spheroids of the HuTu-80 cell line and HT29-MTX-E12 a considerable reduction could also be observed.

3.7. Detection of vital, apoptotic, and necrotic cells

Tumor spheroids of the cell lines HuTu-80 and HT29-MTX-E12 were examined with regard to apoptotic and necrotic effects using FACS analysis. The main reactions triggered by PDT in tumor cells are apoptosis and necrosis. Detection of these events provides information about the cellular composition of vascularized tumor spheroids according to induced phototoxicity. For this purpose, the vascularized tumor spheroids of cell lines HuTu-80 and HT29-MTX-E12 were incubated with free and nanoparticulate photosensitizers on day 12 and the phototoxic effect was induced by irradiation on day 14. On day 17, tumor spheroids were extracted from the CAM, the cells were separated, counted (see 3.6), stained, and measured by FACS analysis. For control purposes, untreated vascularized tumor spheroids were analyzed. The vascularized tumor spheroids of the HuTu-80 cell line had a composition of 90 ± 2% vital, 8 ± 1% apoptotic and 2 ± 0.2% necrotic cells (Fig. 7, A). After the treatment of the tumor spheroids with the free photosensitizer mTHPC, no cells could be detected on the CAM and therefore, no cells were analyzed by FACS. The vascularized tumor spheroids treated with the liposomal formulations show a composition of 85 ± 12% vital, 7 ± 1% apoptotic and 8 ± 6% necrotic cells for LP-BLC 2175 and 25 ± 10% vital, 3 ± 1% apoptotic and 72 ± 11% necrotic cells for LP-BLC 5152. The use of the PLGA-based nanoparticles resulted in 46 ± 9%

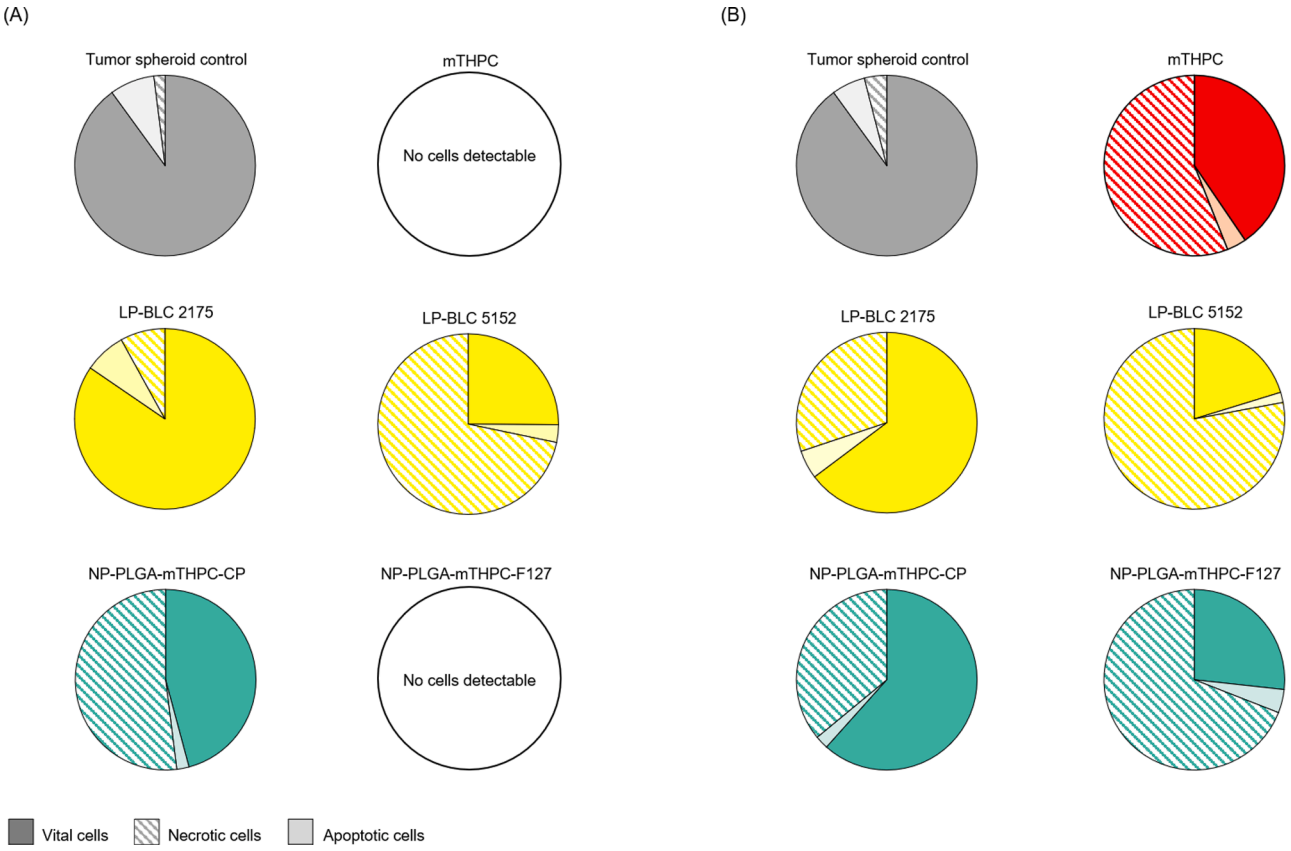

Fig. 7. Detection of apoptosis and necrosis of treated vascularized tumor spheroids of the cell line HuTu-80 and HT29-MTX-E12 Vascularized tumor spheroids of the cell lines (A) HuTu-80 and (B) HT29-MTX-E12 were incubated with the free photosensitizer mTHPC, the liposome-based nanoparticles LP-BLC 2175 and LP-BLC 5152, and the PLGA-based nanoparticles NP-PLGA-mTHPC—CP and NP-PLGA-mTHPC-F127 for 48 h followed by light irradiation. The percentage of vital, apoptotic, and necrotic cells was determined by FACS analysis. The results are presented as mean value. ($n = 4$; k = 4).

vital, 2 ± 1% apoptotic and 52 ± 8% necrotic cells for NP-PLGA-mTHPC—CP. We could not extract enough cells for FACS analysis after the treatment of tumor spheroids from the cell line HuTu-80 with NP-PLGA-mTHPC-F127. Analogous to the treatment of vascularized tumor spheroids of cell line HuTu-80, measurements of apoptotic and necrotic events were performed with treated vascularized tumor spheroids of cell line HT29-MTX-E12 (Fig. 7, B). Cell control measurements revealed a cellular composition of 90 ± 3% vital, 6 ± 1% apoptotic and 4 ± 1% necrotic cells and treatment with the photosensitizer mTHPC resulted in 41 ± 16% vital, 4 ± 1% apoptotic and 56 ± 2% necrotic cells. For the liposomal formulations, a composition of 65 ± 12% vital, 5 ± 1% apoptotic and 30 ± 6% necrotic cells could be detected for LP-BLC 2175 and 20 ± 9% vital, 2 ± 1% apoptotic and 78 ± 10% necrotic cells for LP-BLC 5152. The PLGA-based nanoparticles revealed a cellular composition of tumor spheroids for NP-PLGA-mTHPC—CP of 62 ± 11% vital, 2 ± 1% apoptotic and 36 ± 9% necrotic cells and for NP-PLGA-mTHPC-F127 of 27 ± 9% vital, 4 ± 1% apoptotic and 69 ± 5% necrotic cells. Overall, the results of the investigation of apoptotic and necrotic events of vascularized tumor spheroids of cell lines HuTu-80 and HT29-MTX-E12 showed an increase in necrotic cells after treatment with the free mTHPC and the nanoparticulate formulations of the photosensitizers. This increase is 8 to 72% for the vascularized tumor spheroids of the cell line HuTu-80 and 30 to 69% for the cell line HT29-MTX-E12. As a result, a phototoxic effect, which triggered apoptotic and necrotic events in the vascularized tumor spheroids, was determined.

In PDT, the destruction of tumor cells is accomplished by apoptosis as well as necrosis. Apoptosis is induced in this process by destruction of the mitochondria and the cytoplasm, or by a local undersupply due to damage of blood vessels in the tumor. Necrosis is primarily triggered by destruction of the cell membrane (Mroz et al., 2011). In a study investigating the effect of PDT on P388 and L1210 cells (leukemic cell lines), a concentration-dependent relationship to necrotic and apoptotic processes was established. A low concentration triggered increased cell apoptosis and high concentrations activated necrotic processes (Kessel and Luo, 1998). Based on the present results, it can therefore be assumed that the amount of photosensitizer accumulated in vascularized tumor spheroids was high enough to achieve a notable anti-tumor effect.

The results show that the free photosensitizer mTHPC is a highly effective anti-cancer agent. Direct application of the free photosensitizer to the vascularized tumor spheroids and followed irradiation resulted in complete elimination of tumor cells. Nevertheless, the search for nanoparticulate formulations for effective transport of photosensitizers is an important challenge, due to the limitations of photosensitizers with respect to poor water solubility, long-term phototoxicity and low tumor targeting efficacy (Bae and Na, 2012; Castano et al., 2005; Debele et al., 2015; Park et al., 2018; Zhang et al., 2018). A potential target side for nanoparticulate formulations is the mucus layer which is lining the gastrointestinal tract and the intestine tumors (Bose and Mukherjee, 2020; Hattrup and Gendler, 2008; Kufe, 2009). Modification of the nanoparticulate formulations with Carbopol® should result in improved adhesion of the nanoparticles to the mucus layer of the tumor. Modification with Pluronic® F127 and the use of liposomal formulations should allow permeation across the mucus layer. The duodenum adenocarcinoma cell line HuTu-80 and the human colon cancer cell line HT29-MTX-E12 were used for the generation of tumor spheroids. The HT29-MTX-E12 cell have the specific property to produce mucus (Lozoya-Agullo et al., 2017). In a previous publication we could show that a mucus layer formed on the surface during the generation of the tumor spheroids due to the innovative generation method combining static and dynamic culture conditions. We detected this layer by histological staining with nuclear fast red for the cell nucleus and alcian blue for the acid muco-substances and acetic mucins (Elberskirch et al., 2021). Therefore, adhesion and permeation via the mucus layer into the tumor could be simulated. Comparing the values of the quantification of the accumulated amount of the photosensitizer mTHPC, it is increased by 6% in the tumor spheroids of the cell line HuTu-80 compared to the cell line HT29-MTX-E12. This suggests that the permeation of the photosensitizer through the mucosal barrier of the HT29-MTX-E12 tumor spheroids is reduced. An effective reduction of the tumor cell number could be determined for the free photosensitizer mTHPC as well as for all investigated nanoparticulate formulations. However, the highest reduction of the absolute cell number could be measured after treatment of vascularized tumor spheroids of cell lines HuTu-80 and HT29-MTX-E12 with free photosensitizer mTHPC and the nanoparticulate formulation NP-PLGA-mTHPC-F127. Overall, the NP-PLGA-mTHPC-F127 nanoparticulate formulation exhibits the highest transported amount of photosensitizer to the vascularized tumor spheroid and therefore, could be identified as the most effective transport system in this study.

Both newly synthesized BLCs show a photodynamic activity comparable to that of mTHPC but with different effects. This may be due to their liposomal formulation. The incorporation into a liposomal membrane will change the availability of the substances by rendering their release behavior from the vehicle. PDT with BLC2175 is less effective in HuTu-80 cells compared to HT29-MTX-E12 cells. Further, in HuTu-80 cells the number of apoptotic cells is remarkably high after incubation with liposomal BLC5152, whereas with BLC2175 almost all cells are resistant to PDT-treatment. However, the BLC-substances clearly show different effects, thereby demonstrating the suitability of the test system to differentiate between the substance properties.

4. Conclusion

The need and relevance of new tumor models for anticancer drug screening to overcome the limitations of conventional 2D and 3D culture models have been widely acknowledged. The results presented for the developed HET-CAM assay to study the efficacy of photosensitizers and their nanoparticulate formulations indicate that this assay could function as a link between standardized *in vitro* models and animal models. It is particularly suitable for the study of PDT, as focused irradiation of the tumor is possible, which can reflect endoscopic irradiation *in ovo*. We have shown the possibility to study the accumulation and efficacy of free photosensitizers and their nanoparticulate formulations. The knowledge obtained from these investigations can lead to a reduction or even replacement of animal testing for the investigation of photosensitizers and their nanoparticulate formulations for PDT. Furthermore, the developed vascularized intestinal tumor model is not limited to the use of intestinal tumors, other tumor spheroids or organoids can also be used. Another important aspect is the opportunity for interdisciplinary use involving toxicological pharmaceutical research, tissue engineering and material sciences. Thus, the vascularized intestinal tumor model based on the HET-CAM test presented here opens new possibilities to improve conventional 2D and 3D culture models.

Funding

This work was financially supported by the BMBF (13N13424, 2014).

CRediT authorship contribution statement

Linda Elberskirch: Methodology, Validation, Formal analysis, Investigation, Writing – original draft, Writing – review & editing. **Ronan Le Harzic:** Methodology, Writing – original draft. **Dietrich Scheglmann:** Investigation, Resources. **Gerhard Wieland:** Methodology, Investigation, Writing – review & editing. **Arno Wiehe:** Validation, Investigation, Writing – review & editing. **Maria Mathieu-Gaedke:** Validation, Investigation, Writing – review & editing. **Hartwig R.A. Golf:** Validation, Investigation, Writing – review & editing. **Hagen von Briesen:** Conceptualization, Methodology, Writing – review & editing, Supervision, Project administration, Funding acquisition. **Sylvia Wagner:** Conceptualization, Methodology, Writing – review & editing,

Supervision, Project administration, Funding acquisition.

Declaration of Competing interests

The authors declare no competing or financial interests.

Acknowledgements

We thank Max Sokoli and Marcel Meyerheim for the help during the establishment of the HET-CAM assay.

References

Bae, B.C., Na, K., 2012. Development of polymeric cargo for delivery of photosensitizer in photodynamic therapy. Int. J. Photoenergy. https://doi.org/10.1155/2012/431975.

Betz, C.S., Rauschning, W., Stranadko, E.P., Riabov, M.V., Albrecht, V., Nifantiev, N.E., Hopper, C., 2008. Optimization of treatment parameters for Foscan®-PDT of basal cell carcinomas. Lasers Surg. Med. 40, 300–311. https://doi.org/10.1002/lsm.20632.

Biel, M.A., 2010. Photodynamic therapy of head and neck cancers. Methods Mol. Biol. 635, 281–293. https://doi.org/10.1007/978-1-60761-697-9_18.

Bœuf-Muraille, G., Rigaux, G., Callewaert, M., Zambrano, N., Van Gulick, L., Roullin, V. G., Terryn, C., Andry, M.C., Chuburu, F., Dukic, S., Molinari, M., 2019. Evaluation of mTHPC-loaded PLGA nanoparticles for *in vitro* photodynamic therapy on C6 glioma cell line. Photodiagnosis Photodyn. Ther. 25, 448–455. https://doi.org/10.1016/j.pdpdt.2019.01.026.

Bonnett, R., White, R.D., Winfield, U.J., Berenbaum, M.C., 1989. Hydroporphyrins of the meso-tetra(hydroxyphenyl)porphyrin series as tumour photosensitizers. Biochem. J. 261, 277–280. https://doi.org/10.1042/bj2610277.

Bose, M., Mukherjee, P., 2020. Potential of anti-muc1 antibodies as a targeted therapy for gastrointestinal cancers. Vaccines. https://doi.org/10.3390/vaccines8040659.

Castano, Ana P, Demidova, T.N., Hamblin, M., 2004. Mechanisms in photodynamic therapy: part one - photosensitizers, photochemistry and cellular localization. Photodiagnosis Photodyn. Ther. 1, 279–293. https://doi.org/10.1016/S1572-1000(05)00007-4.Mechanisms.

Castano, A.P., Demidova, T.N., Hamblin, M.R., 2005. Mechanisms in photodynamic therapy: part two - cellular signaling, cell metabolism and modes of cell death. Photodiagnosis Photodyn. Ther. 2, 1–23. https://doi.org/10.1016/S1572-1000(05)00030-X.

Cimpean, A.M., Ribatti, D., Raica, M., 2008. The chick embryo chorioallantoic membrane as a model to study tumor metastasis. Angiogenesis. https://doi.org/10.1007/s10456-008-9117-1.

Cramers, P., Ruevekamp, M., Oppelaar, H., Dalesio, O., Baas, P., Stewart, F.A., 2003. Foscan® uptake and tissue distribution in relation to photodynamic efficacy. Br. J. Cancer 88, 283–290. https://doi.org/10.1038/sj.bjc.6600682.

Debele, T.A., Peng, S., Tsai, H.C., 2015. Drug carrier for photodynamic cancer therapy. Int. J. Mol. Sci. https://doi.org/10.3390/ijms160922094.

Demir, R., Dimmler, A., Naschberger, E., Demir, I., Papadopoulos, T., Melling, N., Sturzl, M., Hohenberger, W., 2009. Malignant progression of invasive tumour cells seen in hypoxia present an accumulation of β-catenin in the nucleus at the tumour front. Exp. Mol. Pathol. 87, 109–116. https://doi.org/10.1016/j.yexmp.2009.05.004.

Dewhirst, M.W., Secomb, T.W., 2017. Transport of drugs from blood vessels to tumour tissue. Nat. Rev. Cancer. https://doi.org/10.1038/nrc.2017.93.

Dinakaran, D., Sengupta, J., Pink, D., Raturi, A., Chen, H., Usmani, N., Kumar, P., Lewis, J.D., Narain, R., Moore, R.B., 2020. PEG-PLGA nanospheres loaded with nanoscintillators and photosensitizers for radiation-activated photodynamic therapy. Acta Biomater 117, 335–348. https://doi.org/10.1016/j.actbio.2020.09.029.

Elberskirch, L., Knoll, T., Königsmark, R., Renner, J., Wilhelm, N., von Briesen, H., Wagner, S., 2021. Microfluidic 3D intestine tumor spheroid model for efficient *in vitro* investigation of nanoparticular formulations. J. Drug Deliv. Sci. Technol. 63, 102496 https://doi.org/10.1016/j.jddst.2021.102496.

Friedrich, J., Seidel, C., Ebner, R., Kunz-Schughart, L.A., 2009. Spheroid-based drug screen: considerations and practical approach. Nat. Protoc. 4, 309–324. https://doi.org/10.1038/nprot.2008.226.

Graham, M.L., Prescott, M.J., 2015. The multifactorial role of the 3Rs in shifting the harm-benefit analysis in animal models of disease. Eur. J. Pharmacol. 759, 19–29. https://doi.org/10.1016/j.ejphar.2015.03.040.

Hattrup, C.L., Gendler, S.J., 2008. Structure and function of the cell surface (tethered) mucins. Annu. Rev. Physiol. https://doi.org/10.1146/annurev.physiol.70.113006.100659.

Hornung, R., Fehr, M.K., Walt, H., Wyss, P., Berns, M.W., Tadir, Y., 2004. PEG-m-THPC–mediated photodynamic effects on normal rat tissues¶. Photochem. Photobiol. 72, 696. https://doi.org/10.1562/0031-8655(2000)072<0696:pmtmpe>2.0.co;2.

Katsen-Globa, A., Puetz, N., Gepp, M.M., Neubauer, J.C., Zimmermann, H., 2016. Study of SEM preparation artefacts with correlative microscopy: cell shrinkage of adherent cells by HMDS-drying. Scanning 38, 625–633. https://doi.org/10.1002/sca.21310.

Katsen, A.D., Vollmar, B., Mestres-Ventura, P., Menger, M.D., 1998. Cell surface and nuclear changes during TNF-α-induced apoptosis in WEHI 164 murine fibrosarcoma cells. A correlative light, scanning, and transmission electron microscopical study. Virchows Arch 433, 75–83. https://doi.org/10.1007/s004280050219.

Kessel, D., Luo, Y., 1998. Mitochondrial photodamage and PDT-induced apoptosis. J. Photochem. Photobiol. B Biol. 42, 89–95. https://doi.org/10.1016/S1011-1344(97)00127-9.

Kiesslich, T., Berlanda, J., Plaetzer, K., Krammer, B., Berr, F., 2007. Comparative characterization of the efficiency and cellular pharmacokinetics of Foscan®- and Foslip®-based photodynamic treatment in human biliary tract cancer cell lines. Photochem. Photobiol. Sci. 6, 619–627. https://doi.org/10.1039/b617659c.

Kufe, D.W., 2009. Mucins in cancer: function, prognosis and therapy. Nat. Rev. Cancer. https://doi.org/10.1038/nrc2761.

Langhans, S.A., 2018. Three-dimensional *in vitro* cell culture models in drug discovery and drug repositioning. Front. Pharmacol. 9, 6. https://doi.org/10.3389/fphar.2018.00006.

Lebelt, A., Dziecioł, J., Guzińska-Ustymowicz, K., Lemancewicz, D., Zimnoch, L., Czykier, E., 2008. Angiogenesis in gliomas. Folia Histochem. Cytobiol. 46, 69–72. https://doi.org/10.2478/v10042-008-0009-4.

Li, W.W., Li, V.W., Hutnik, M., Chiou, A.S., 2012. Tumor angiogenesis as a target for dietary cancer prevention. J. Oncol. https://doi.org/10.1155/2012/879623.

Lokman, N.A., Elder, A.S.F., Ricciardelli, C., Oehler, M.K., 2012. Chick chorioallantoic membrane (CAM) assay as an *in vivo* model to study the effect of newly identified molecules on ovarian cancer invasion and metastasis. Int. J. Mol. Sci. 13, 9959–9970. https://doi.org/10.3390/ijms13089959.

Lou, P.J., Jones, L., Hopper, C., 2003. Clinical outcomes of photodynamic therapy for head-and-neck cancer. Technol. Cancer Res. Treat. https://doi.org/10.1177/153303460300200405.

Lovitt, C.J., Shelper, T.B., Avery, V.M., 2014. Advanced cell culture techniques for cancer drug discovery. Biology (Basel) 3, 345–367. https://doi.org/10.3390/biology3020345.

Lozoya-Agullo, I., Araújo, F., González-Álvarez, I., Merino-Sanjuán, M., González-Álvarez, M., Bermejo, M., Sarmento, B., 2017. Usefulness of Caco-2/HT29-MTX and Caco-2/HT29-MTX/Raji B coculture models to predict intestinal and colonic permeability compared to Caco-2 monoculture. Mol. Pharm. 14, 1264–1270. https://doi.org/10.1021/acs.molpharmaceut.6b01165.

Ma, L., Moan, J., Berg, K., 1994. Evaluation of a new photosensitizer, meso-tetra-hydroxyphenyl-chlorin, for use in photodynamic therapy: a comparison of its photobiological properties with those of two other photosensitizers. Int. J. Cancer 57, 883–888. https://doi.org/10.1002/ijc.2910570618.

Manjunathan, R., Ragunathan, M., 2015. Chicken chorioallantoic membrane as a reliable model to evaluate osteosarcoma - An experimental approach using SaOS2 cell line. Biol. Proced. Online 17, 1–13. https://doi.org/10.1186/s12575-015-0022-x.

Mohs, R.C., Greig, N.H., 2017. Drug discovery and development: role of basic biological research. Alzheimer's Dement. Transl. Res. Clin. Interv. 3, 651–657. https://doi.org/10.1016/j.trci.2017.10.005.

Mokwena, M.G., Kruger, C.A., Ivan, M.T., Heidi, A., 2018. A review of nanoparticle photosensitizer drug delivery uptake systems for photodynamic treatment of lung cancer. Photodiagnosis Photodyn. Ther. https://doi.org/10.1016/j.pdpdt.2018.03.006.

Mroz, P., Yaroslavsky, A., Kharkwal, G.B., Hamblin, M.R., 2011. Cell death pathways in photodynamic therapy of cancer. Cancers (Basel). https://doi.org/10.3390/cancers3022516.

Nath, S., Devi, G.R., 2016. Three-dimensional culture systems in cancer research: focus on tumor spheroid model. Pharmacol. Ther. https://doi.org/10.1016/j.pharmthera.2016.03.013.

Niu, X., Zou, W., Liu, C., Zhang, N., Fu, C., 2009. Modified nanoprecipitation method to fabricate DNA-loaded PLGA nanoparticles modified nanoprecipitation method. Drug Dev. Ind. Pharm. 35, 1375–1383. https://doi.org/10.3109/03639040902939221.

Nowak-Sliwinska, P., Segura, T., Iruela-Arispe, M.L., 2014. The chicken chorioallantoic membrane model in biology, medicine and bioengineering. Angiogenesis. https://doi.org/10.1007/s10456-014-9440-7.

Park, W., Cho, S., Han, J., Shin, H., Na, K., Lee, B., Kim, D.H., 2018. Advanced smart-photosensitizers for more effective cancer treatment. Biomater. Sci. 6, 79–90. https://doi.org/10.1039/c7bm00872d.

Ribatti, D., Gualandris, A., Bastaki, M., Vacca, A., Iurlaro, M., Roncali, L., Presta, M., 1997. New model for the study of angiogenesis and antiangiogenesis in the chick embryo chorioallantoic membrane: the gelatin sponge/chorioallantoic membrane assay. J. Vasc. Res. 34, 455–463. https://doi.org/10.1159/000159256.

Rojnik, M., Kocbek, P., Moret, F., Compagnin, C., Celotti, L., Bovis, M.J., Woodhams, J. H., MacRobert, A.J., Scheglmann, D., Helfrich, W., Verkaik, M.J., Papini, E., Reddi, E., Kos, J., 2012. *In vitro* and *in vivo* characterization of temoporfin-loaded PEGylated PLGA nanoparticles for use in photodynamic therapy. Nanomedicine 7, 663–677. https://doi.org/10.2217/nnm.11.130.

Russell, W., Burch, R., 1959. The principles of humane experimental technique.

Sausville, E.A., Newell, D.R., 2004. Preclinical models in cancer drug discovery and development. Eur. J. Cancer. https://doi.org/10.1016/j.ejca.2004.01.010.

Shu, M., Tang, J., Chen, L., Zeng, Q., Li, C., Xiao, S., Jiang, Z., Liu, J., 2021. Tumor microenvironment triple-responsive nanoparticles enable enhanced tumor penetration and synergetic chemo-photodynamic therapy. Biomaterials 268. https://doi.org/10.1016/j.biomaterials.2020.120574.

Subauste, C.M., Kupriyanova, T.A., Conn, E.M., Ardi, V.C., Quigley, J.P., Deryugina, E.I., 2009. Evaluation of metastatic and angiogenic potentials of human colon carcinoma cells in chick embryo model systems. Clin. Exp. Metastasis 26, 1033–1047. https://doi.org/10.1007/s10585-009-9293-4.

Swadi, R., Mather, G., Pizer, B.L., Losty, P.D., See, V., Moss, D., 2018. Optimising the chick chorioallantoic membrane xenograft model of neuroblastoma for drug delivery. BMC Cancer 18. https://doi.org/10.1186/s12885-017-3978-x.

Vargas, A., Zeisser-Labouèbe, M., Lange, N., Gurny, R., Delie, F., 2007. The chick embryo and its chorioallantoic membrane (CAM) for the *in vivo* evaluation of drug delivery systems. Adv. Drug Deliv. Rev. https://doi.org/10.1016/j.addr.2007.04.019.

Vu, B.T., Shahin, S.A., Croissant, J., Fatieiev, Y., Matsumoto, K., Le-Hoang Doan, T., Yik, T., Simargi, S., Conteras, A., Ratliff, L., Jimenez, C.M., Raehm, L., Khashab, N., Durand, J.O., Glackin, C., Tamanoi, F., 2018. Chick chorioallantoic membrane assay as an *in vivo* model to study the effect of nanoparticle-based anticancer drugs in ovarian cancer. Sci. Rep. 8, 1–10. https://doi.org/10.1038/s41598-018-25573-8.

Xiao, X., Zhou, X., Ming, H., Zhang, J., Huang, G., Zhang, Z., Li, P., 2015. Chick chorioallantoic membrane assay: a 3D animal model for study of human nasopharyngeal carcinoma. PLoS ONE 10, e0130935. https://doi.org/10.1371/journal.pone.0130935.

Xu, Q., Boylan, N.J., Cai, S., Miao, B., Patel, H., Hanes, J., 2013. Scalable method to produce biodegradable nanoparticles that rapidly penetrate human mucus. J. Control. Release 170, 279–286. https://doi.org/10.1016/j.jconrel.2013.05.035.

Yakavets, I., Millard, M., Zorin, V., Lassalle, H.P., Bezdetnaya, L., 2019. Current state of the nanoscale delivery systems for temoporfin-based photodynamic therapy: advanced delivery strategies. J. Control. Release. https://doi.org/10.1016/j.jconrel.2019.05.035.

Zabielska-Koczywas, K., Wojtkowska, A., Dolka, I., Małek, A., Walewska, M., Wojtalewicz, A., Zbikowski, A., Lechowski, R., 2017. 3D chick embryo chorioallantoic membrane model as an *in vivo* model to study morphological and histopathological features of feline fibrosarcomas. BMC Vet. Res. 13, 1–12. https://doi.org/10.1186/s12917-017-1114-4.

Zhang, J., Jiang, C., Figueiró Longo, J.P., Azevedo, R.B., Zhang, H., Muehlmann, L.A., 2018. An updated overview on the development of new photosensitizers for anticancer photodynamic therapy. Acta Pharm. Sin. B. https://doi.org/10.1016/j.apsb.2017.09.003.